Electronic Supporting Information

for

An unsymmetrical pentacene derivative with ambipolar behavior in organic thin-film transistors

Sebastian H. Etschel,[a,b] Andreas R. Waterloo,[a] Johannes T. Margraf,[c] Atefeh Y. Amin,[b] Frank Hampel,[a] Christof M. Jäger,[c] Timothy Clark,[c] Marcus Halik,*[b] and Rik R. Tykwinski*[a]

[a] *Friedrich-Alexander-Universität Erlangen-Nürnberg, Department of Chemistry and Pharmacy & Interdisciplinary Center of Molecular Materials (ICMM), Henkestraße 42, 91054 Erlangen, Germany. Fax: +49 9131 – 85 26 865; Tel: +49 9131 – 85 22 540; E-Mail: rik.tykwinski@chemie.uni-erlangen.de*

[b] *Friedrich-Alexander-Universität Erlangen-Nürnberg, Institute of Polymer Materials, Organic Materials and Devices, Martensstraße 7, 91058 Erlangen, Germany. Fax: +49 9131 – 85 28 321; Tel: +49 9131 – 85 27 732; E-Mail: marcus.halik@ww.uni-erlangen.de*

[c] *Friedrich-Alexander-Universität Erlangen-Nürnberg, Computer Chemie Centrum, Nägelsbachstraße 25, 91052 Erlangen, Germany. Fax: +49 9131 – 85 26 565; Tel: +49 9131 – 85 22 948; E-Mail: clark@chemie.uni-erlangen.de*

Table of Contents for the Electronic Supporting Information:

1. General Experimental

a) Chemicals: All chemicals were purchased from commercial suppliers and used as received. THF and Et_2O were distilled from sodium/benzophenone, prior to use. Analytical TLC was performed on Al plates coated with 0.20 mm silica gel and containing a fluorescent indicator (Macherey-Nagel, ALUGRAM® SIL G/UV_{254}). Column chromatography was carried out on silica gel (Macherey-Nagel, M-N Silica Gel 60A, 230–400 mesh). The Mo boats and W coils for the deposition of the corresponding material were used as received (Umicore). Al (ChemPur) and Au (ESG GmbH & Co. -KG) for the transistor electrodes were used as received.

b) Instrumentation: Melting points are uncorrected and were determined by a Electrothermal melting point apparatus model 9100. UV–vis characterization was performed on a Cary 5000 UV–vis–NIR (Varian) spectrometer. Fluorescence spectra were obtained at a Fluoromax–4 Spectrofluorometer (Horiba Jobin Yvon). IR spectra were recorded on a Varian 660-IR (ATR mode) spectrometer. Characteristic IR bands were recorded in cm^{-1} and classified as strong (s), medium (m), and weak (w). ^{1}H, ^{13}C, and ^{19}F NMR spectra were recorded on a Bruker Avance 300 spectrometer. ^{1}H and ^{13}C NMR spectra were referenced to the residual solvent signal (^{1}H: $CDCl_3$, δ = 7.24 ppm, ^{13}C: $CDCl_3$, δ = 77.0 ppm) and recorded at ambient conditions. Mass spectra were obtained by a MicroOTOF II (Bruker, ESI-HRMS) or a maXis 4G (Bruker, APPI HRMS). TGA was performed by a Perkin Elmer Pyris 1 TGA instrument. DSC was carried out at a Perkin Elmer Pyris 1 DSC instrument. All thermal analyses were carried out under a flow of nitrogen with a heating rate of 10 °C/min. Thermal decomposition temperature as measured by TGA, indicated by the sample weight loss, are reported as T_d in which the reported temperature corresponds to the intersection of the intersection of the tangent lines of the baseline and the edge of the peak corresponding to the first significant weight loss (> 5%). Melting points from DSC were reported as *M*p and referred to the maximum of the first endothermic energy uptake. In cases, where decomposition takes place, the onset and maximum of the exothermic decomposition peak is reported. Cyclic voltammetry was carried out, using a BASi Voltammetric Analyzer CV–50W. Atomic Force Microscopy was carried out in the tapping mode on a Vecco NanoMan VS atomic force microscope.

X-ray data for **1a** (CCDC 927705), **1b** (CCDC 927706), and **1c** (CCDC 927707) have been deposited at the Cambridge Crystallographic Data Centre (CCDC), 12 Union Road, Cambridge CB2 1EZ, UK, telephone: +44 1223 336408, fax: +44 1223 336033; These data can be obtained free of charge from the Cambridge Crystallographic Data Centre *via* the internet at www.ccdc.cam.ac.uk/data_request/cif using the CCDC numbers given above. Alternatively, X-ray data of **1a**, **1b**, and **1c** is available from the author, or Dr. Frank Hampel, X-ray Crystallographic Lavatory of the Institute for Organic Chemistry, University of Erlangen-Nuremberg, Henkestraße 42, 91054 Erlangen, Germany. (xray.oc@chemie.uni-erlangen.de)

2. Synthetic Procedures and Spectral Characterization of Compounds 1a–c, 2b, and 3a,b

a) General Procedure for compounds 1a–c

Unless indicated otherwise, to a solution of the corresponding anthracene **2a** or **2b** (3 equiv.) in dry THF (20 mL), *n*-BuLi (2.9 equiv., 2.5 M in hexanes) was added under N_2 atmosphere at –78 °C. The mixture was stirred for 30 min at that temperature, before the corresponding ketone **3a** or **3b** (1 equiv.) was added as a solid. The resulting suspension was stirred for 14–16 h at rt under N_2 atmosphere. The reaction was quenched *via* addition of satd. aq. NH_4Cl (50 mL) and extracted with CH_2Cl_2 (3 x 50 mL). The organic phases were combined, washed with brine (100 mL), dried (Na_2SO_4), filtered, and the solvent removed *in vacuo*. The resulting residue was dissolved in dry THF (20 mL) and submitted to reductive aromatization *via* addition of $SnCl_2{\cdot}2H_2O$ (3 equiv.) and 10% aq. H_2SO_4 (0.5–1 mL). The mixture was protected from light and stirred for 4–6 h. The reaction was quenched *via* addition of satd. aq. NH_4Cl (50 mL) and extracted with CH_2Cl_2 (3 x 50 mL). For better phase separation, 1–5 mL of concentrated HCl were added. The combined organic phases were washed with brine (100 mL), dried (Na_2SO_4), filtered, and the solvent removed *in vacuo*. The crude product was separated using column chromatography (silica gel). The crude product was brought onto the column, using hexanes/CH_2Cl_2 (5/1) and the eluent was then changed to hexanes. The first two fluorescent bands were then eluted. The eluent was changed to hexanes/CH_2Cl_2 (5/1), and the product was collected as the deep blue band. The solvent was removed *in* vacuo and the obtained blue solid was purified by recrystallization from CH_2Cl_2 layered with MeOH at –15 °C to afford compounds **1a–c** each as a blue solid.

b) 9-bromo-10-fluoroanthracene – 2b

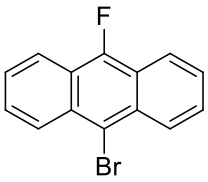

Synthesis, spectral, and physical data were consistent with those reported.[1]

c) 13-hydroxy-13-((triisopropylsilyl)ethynyl)pentacen-6-one – 3a

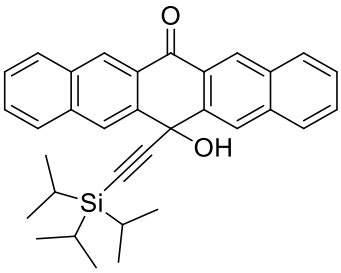

Synthesis, spectral, and physical data were consistent with those reported.[2]

d) 13-hydroxy-13-((triisobutylsilyl)ethynyl)pentacen-6-one – 3b

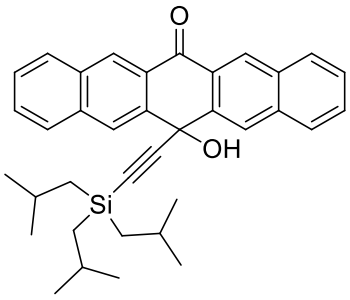

Synthesis, spectral, and physical data were consistent with those reported.[2]

e) (13-(anthracen-9-yl)-6-ethynyl-triisopropylsilyl)-pentacene – 1a

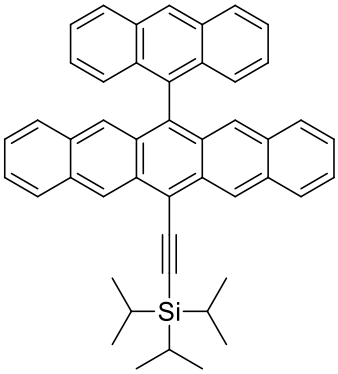

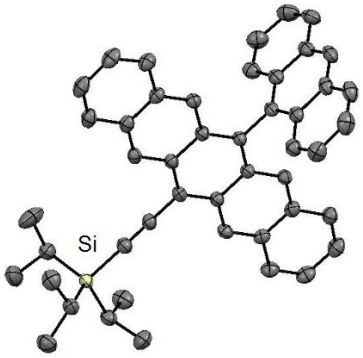

9-Bromoanthracene (0.771 g, 3.00 mmol), *n*-BuLi (2.5 M in hexanes, 1.2 mL, 2.9 mmol), and ketone **3a** (0.491 g, 1.00 mmol) in dry THF (20 mL) were subjected to the General Procedure. Reductive aromatization was performed with $SnCl_2{\cdot}2H_2O$ (0.677 g, 3.00 mmol) and 10% aq. H_2SO_4 (1 mL). Purification was achieved by column chromatography (silica gel, hexanes/CH_2Cl_2 5/1) and recrystallization from CH_2Cl_2 layered with MeOH at −15 °C. Pentacene **1a** was obtained as a blue solid (326 mg, 51%). *Mp* = 306–308 °C; R_f = 0.45 (hexanes/CH_2Cl_2, 5/1); UV/Vis (CH_2Cl_2) λ_{max} (ε): 227 (31 000), 256 (113 600), 300 (81 300), 310 (250 000), 331 (9 000), 349 (11 300), 367 (10 200), 387 (8 600), 435 (1 900), 535 (3 800), 576 (8 500), 623 (13 800); Fluorescence (CH_2Cl_2, λ_{exc} = 615 nm): $\lambda_{max,\ em}$ = 650 nm; IR (ATR): 3042 (w), 2936 (m), 2857 (s), 2130 (m), 1457 (s), 1324 (s), 872 (s), 724 (s) cm^{-1}; ^1H NMR (300 MHz, $CDCl_3$): δ = 9.48 (s, 2H), 8.79 (s, 1H), 8.21 (d, J = 8.4 Hz, 2H), 7.96 (d, J = 8.7 Hz, 2H), 7.72 (s, 2H), 7.47–7.42 (m, 2H), 7.37 (d, J = 8.7 Hz, 2H), 7.32–7.27 (m, 2H), 7.15–7.06 (m, 6H), 1.43 (bs, 21H); ^{13}C NMR (100.5 MHz, $CDCl_3$): δ = 135.0, 133.2, 132.1, 131.9, 131.72, 131.66, 131.1, 129.7, 128.64, 128.57, 128.5, 127.6, 127.0, 126.2, 126.1, 126.0, 125.9, 125.4, 125.3, 118.0, 105.8, 104.9, 19.1, 11.8; APPI HRMS *m/z* calc. $C_{47}H_{42}Si$ 634.3050 (M^+), found 634.3048; TGA: T_d = 297 °C; DSC: 194 (onset), 197 (peak).

A crystal suitable for X-ray crystallographic analysis has been grown by slow evaporation of a CH_2Cl_2 solution layered with MeOH at 4 °C. X-ray data for **1a** ($C_{47}H_{42}Si$), F_w = 634.90; monoclinic crystal system; space group $P2_1/c$; crystal dimensions 0.443 x 0.166 x 0.153 mm^3; a = 7.6889(3) Å, b = 31.5880(11) Å, c = 14.4774(4) Å; β = 91.378(4)°; V = 3515.2(2) $Å^3$; Z = 4; ρ_{calc} = 1.200 g/cm^3; $2\Theta_{max}$ = 147.1°; μ = 0.822 mm^{-1}; T = 173.0 K; total data collected = 12209; R_1 = 0.0510; wR_2 = 0.1918 for 6732 observed reflections and 439 variables; residual electron density = 0.459 and –0.376 $eÅ^{-3}$.

f) (13-(anthracen-9-yl)-6-ethynyl-triisobutylsilyl)-pentacene – 1b

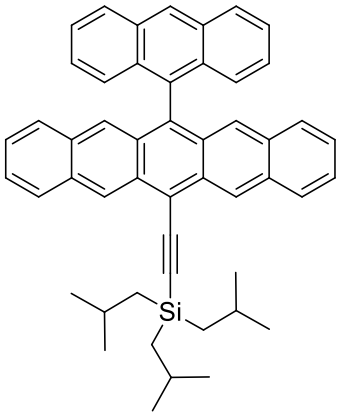

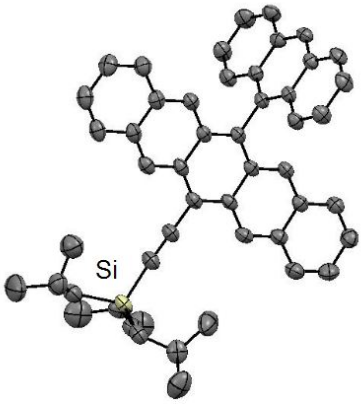

9-Bromoanthracene (0.386 g, 1.50 mmol), *n*-BuLi (2.5 M in hexanes, 0.58 mL, 1.5 mmol), and ketone **3b** (0.268 g, 0.503 mmol) in dry THF (20 mL) were subjected to the General Procedure. Reductive aromatization was performed with $SnCl_2{\cdot}2H_2O$ (0.339 g, 1.50 mmol) and 10% aq. H_2SO_4 (0.5 mL). Purification was achieved by column chromatography according to the General Procedure and recrystallization from CH_2Cl_2 layered with MeOH at −15 °C. Pentacene **1b** was obtained as a blue solid (71 mg, 20%). *Mp* = 277 °C; R_f = 0.38 (silica gel; hexanes/CH_2Cl_2 5/1); R_f = 0.11 (silica gel; hexanes); UV-vis (CH_2Cl_2) λ_{max} (ε) 228 (37 000), 256 (128 600), 300 (94 800), 310 (287 700), 349 (14 000), 367 (12 300), 387 (10 100), 435 (2 355), 536 (4 524), 575 (10 200), 623 (16 400); Fluorescence (CH_2Cl_2, λ_{exc} = 615 nm): $\lambda_{max,\ em}$ = 648 nm; IR (ATR): 3043 (m), 2947 (m), 2921 (m), 2861 (s), 2127 (m), 1588 (w), 1457 (m), 1379 (m), 875 (s), 731 (s) cm^{-1}; ^1H NMR (300 MHz, $CDCl_3$) δ = 9.42 (s, 2H), 8.79 (s, 1H), 8.21 (d, *J* = 8.4 Hz, 2H), 7.94 (d, *J* = 8.7 Hz, 2H), 7.69 (s, 2H), 7.47–7.41 (m, 2H), 7.37 (d, *J* = 8.7 Hz, 2H), 7.31–7.26 (m, 2H), 7.14–7.01 (m, 6H), 2.27 (non, *J* = 6.6 Hz, 3H), 1.25 (d, *J* = 6.3 Hz, 18H), 1.01 (d, *J* = 7.2 Hz, 6H); ^{13}C NMR (75.7 MHz, $CDCl_3$) δ = 134.9, 133.2, 132.1, 131.9, 131.7, 131.6, 131.1, 129.6, 128.64, 128.55, 128.3, 127.6, 126.9, 126.1, 126.00, 125.97, 125.88, 125.4, 125.3, 118.0, 108.5, 104.8, 26.6, 25.5 (one signal coincident or not observed); APPI HRMS calcd for $C_{50}H_{48}Si$ (M^+) 676.3520, found 676.3521; TGA: T_d = 327 °C; DSC: *Mp* = 292 °C, decomposition, 294 °C (onset), 296 °C (peak).

A crystal suitable for X-ray crystallographic analysis has been grown by slow evaporation of a saturated solution of **1b** in CH_2Cl_2 layered with MeOH at 4 °C. X-ray data for **1b** ($C_{50}H_{48}Si$); F_w = 676.97; triclinic crystal system; space group $P\bar{1}$; crystal dimensions 0.334 x 0.166 x 0.062 mm^3; *a* = 9.2544(2) Å, *b* = 18.2908(5) Å, *c* = 24.1358(5) Å, α = 90.662(2)°, β = 98.7052(19)°, γ = 103.547(2)°, *V* = 3921.36(16) $Å^3$; Z = 4; ρ_{calc} = 1.147 g/cm^3; $2\theta_{max}$ = 125.16°; *T* = 173.00(10) K; μ = 0.765 mm^{-1}; total data collected = 18734; R_1 = 0.0794; wR_2 = 0.2239 for 11951 observed reflections 963 variables and 23 restraints; residual electron density = 0.97 and −0.68 $eÅ^{-3}$; Si1-unit: Disorder of all three *iso*-butyl-groups: 58:42 occupation; Si1'-unit: Disorder of one *iso*-butyl-group: C7'/8'/10' : C7a'/8a'/1'' 69:31 occupation.

g) (13-(10-fluoroanthracen-9-yl)-6-ethynyl-triisopropylsilyl)-pentacene – 1c

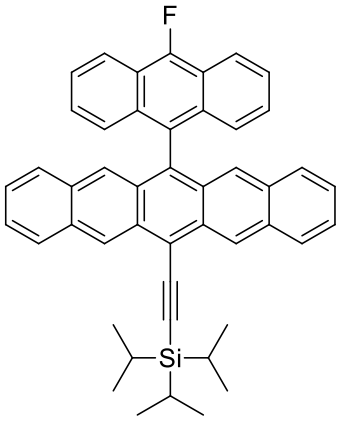

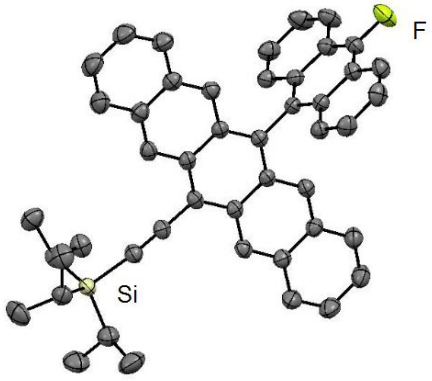

9-Bromo-10-fluoroanthracene **2b** (0.671 g, 2.40 mmol), *n*-BuLi (2.5 M in hexanes, 0.95 mL, 2.3 mmol), and ketone **3a** (0.392 g, 0.798 mmol) in dry THF (20 mL) were subjected to the General Procedure. Reductive aromatization was performed with $SnCl_2{\cdot}2H_2O$ (0.541 g, 2.40 mmol) and 10% aq. H_2SO_4 (0.5 mL). Purification was achieved by column chromatography according to the General Procedure and recrystallization from CH_2Cl_2 layered with MeOH at −15 °C. Pentacene **1c** was obtained as a blue solid (205 mg, 39%). *Mp* = 300 °C; R_f = 0.57 (silica gel; hexanes/CH_2Cl_2 5/1); R_f = 0.09 (silica gel; hexanes); UV-vis (CH_2Cl_2) λ_{max} (ε) 228 (37 000), 257 (176 400), 300 (126 900), 310 (318 400), 352 (14 800), 373 (12 900), 394 (10 400), 435 (2 315), 535 (3 800), 574 (13 300), 622 (22 100); Fluorescence (CH_2Cl_2, λ_{exc} = 615 nm): $\lambda_{max,\ em}$ = 642 nm; IR (ATR): 3047 (m), 2935 (s), 2861 (s), 2131 (m), 1558 (w), 1378 (w), 1341 (s), 871 (s), 734 (s) cm^{-1}; ^1H NMR (300 MHz, $CDCl_3$) δ = 9.45 (s, 2H), 8.48 (d, *J* = 8.7 Hz, 2H), 7.95 (d, *J* = 8.4 Hz, 2H), 7.70 (s, 2H), 7.52–7.47 (m, 2H), 7.41 (d, *J* = 8.7 Hz, 2H), 7.32–7.27 (m, 2H), 7.16–7.00 (m, 6H), 1.42 (bs, 21H); ^{13}C NMR (100.5 MHz, $CDCl_3$) δ = 154.7 (d, $^1J_{C,F}$ = 258 Hz), 134.1, 132.14, 132.11, 131.8, 131.0, 129.9, 128.6, 128.5, 128.4, 126.7 (d, $J_{C,F}$ = 2.7 Hz), 126.6, 126.1, 126.0, 125.9, 125.6 (d, $J_{C,F}$ = 1.9 Hz), 125.4, 120.8 (d, $J_{C,F}$ = 5.5 Hz), 119.2 (d, $J_{C,F}$ = 14.8 Hz), 118.2, 105.9, 104.8, 19.0, 11.7; ^{19}F NMR (282 MHz, $CDCl_3$) δ = −129.5; APPI HRMS calcd for $C_{47}H_{42}FSi$ $[(M + H)]^+$ 653.3033, found 653.3034; $C_{47}H_{41}FSi$ (M^+) 652.2956, found 652.2958; TGA: T_d = 295 °C; DSC: *Mp* = 220 °C.

A crystal suitable for X-ray crystallographic analysis has been grown by slow evaporation of a saturated solution of **1c** in CH_2Cl_2 layered with MeOH at 4 °C. X-ray data for **1c** ($C_{47}H_{41}FSi$), F_w = 652.89; triclinic crystal system; space group P−1 crystal dimensions 0.222 x 0.140 x 0.062 mm^3; *a* = 12.5164(9) Å, *b* = 12.9102(10) Å, *c* = 13.3024(11) Å, α = 85.827(7)°, β = 62.967(8)°, γ = 72.234(7)°, *V* = 1817.9(2) $Å^3$; *Z* = 2; ρ_{calc} = 1.193 g/cm^3; $2\theta_{max}$ = 141.76°; *T* = 173.0(2) K; μ = 0.849 mm^{-1}; total data collected = 10315, R_1 = 0.053; wR_2 = 0.1904 for 6670 observed reflections and 448 variables; residual electron density = 0.37 and −0.31 $eÅ^{-3}$.

3. UV–vis Absorption and Emission Spectra of Compounds 1a–c

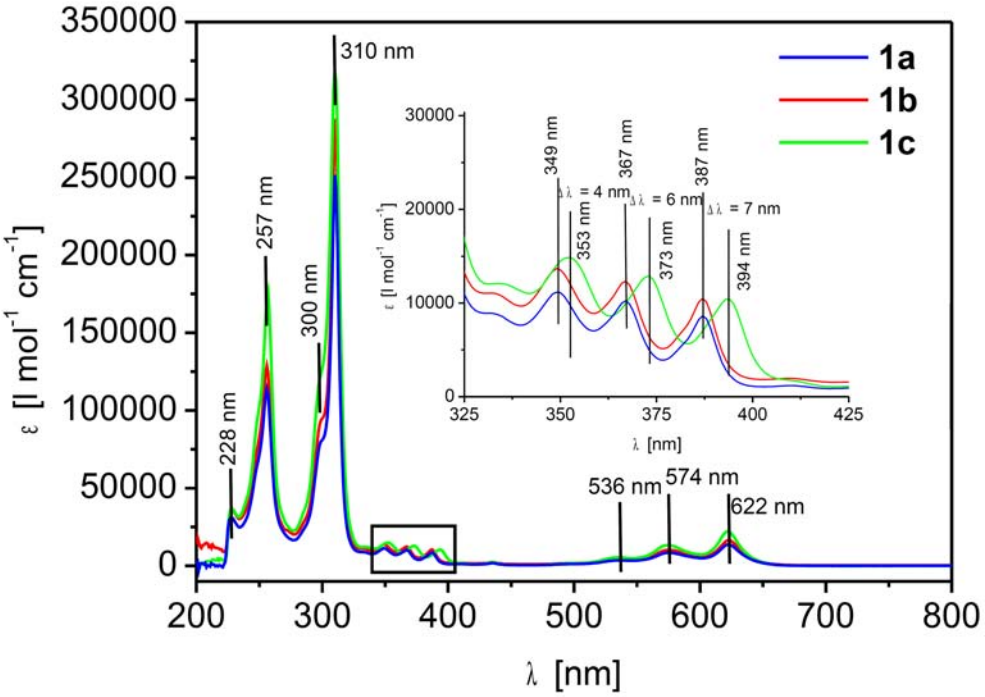

Figure S1: UV–vis spectra of 1a–c, inset shows magnified region between 300 nm and 400 nm.

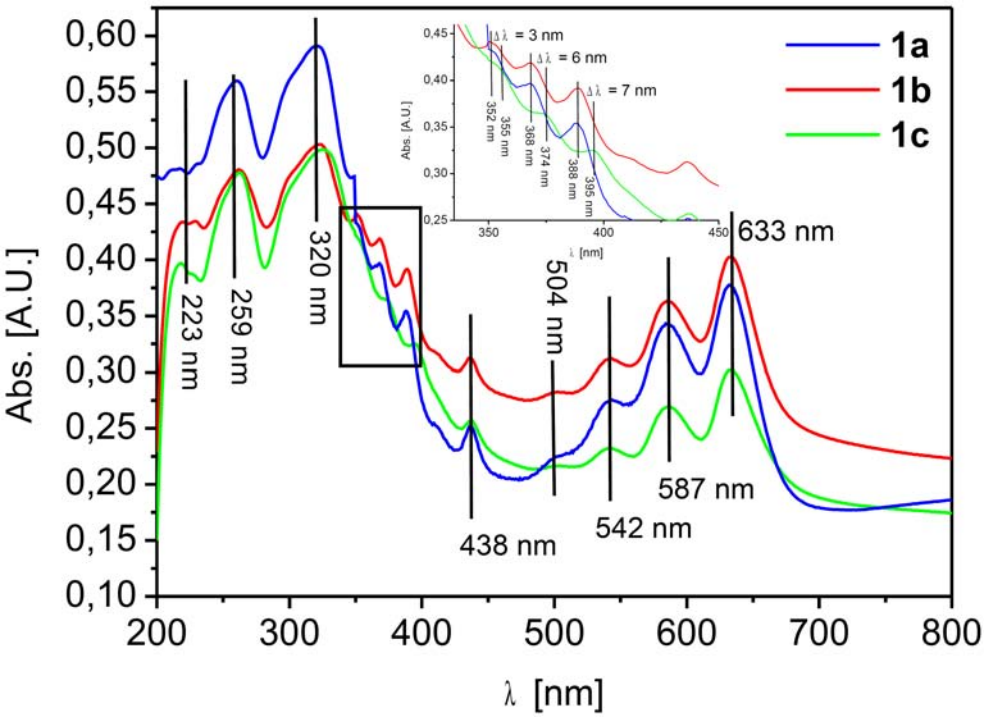

Figure S2: Thin film UV–vis spectra of 1a–c; films were obtained by evaporating CH_2Cl_2 from a 7.5 mM solution of 1a–c.

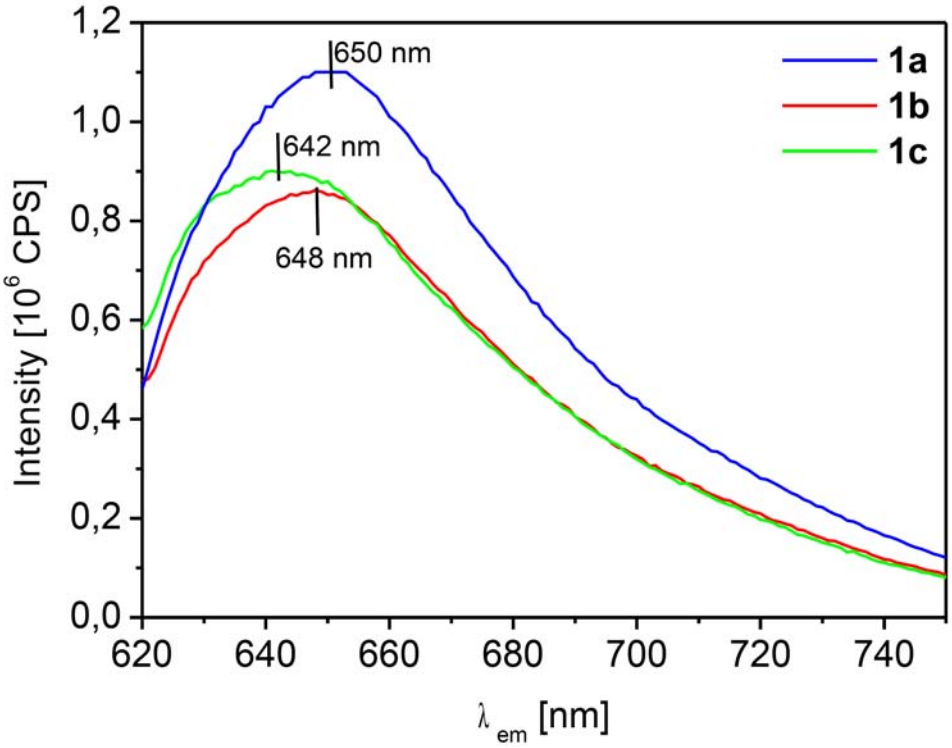

Figure S3: Fluorescence spectra of 1a–c; λ_{exc} = 615 nm.

The optical band gap ($E_{\mathrm{gap}}^{\mathrm{opt}}$) was determined from the offset of longest wavelength absorption peak ($\lambda_{\mathrm{max}}^{\mathrm{off}}$) according to the following equation:

$$E_{\mathrm{gap}}^{\mathrm{opt}} = \frac{h \cdot c}{\lambda_{\mathrm{max}}^{\mathrm{off}}}$$

The offset of the longest wavelength absorption peak ($\lambda_{\mathrm{max}}^{\mathrm{off}}$) was determined by the intercept of the tangent, applied to the longest wavelength absorption peak, and the baseline of the absorption spectrum.

4. Cyclic Voltammetry Data for Compounds 1a–c

Cyclic voltammetry of Compounds **1a–c** was measured in a 0.1 M solution of *n*-Bu_4NPF_6 in CH_2Cl_2, with a platinum working electrode, a platinum counter electrode, and an Ag/AgCl reference electrode. The cyclovotamogramms were recorded from –1.5 V to 1.5 V (*vs.* Ag/AgCl) with a scan rate of 60 mV s^{-1}. The concentration of compounds **1a–c** is stated in the caption of the corresponding cyclovotamogramm. All solutions were degased with N_2 before and were layered with N_2 during measurement. The HOMO and LUMO energies were calculated with the empirical relation:[3]

$$E_{\mathrm{HOMO}} \approx -(E_{1/2}^{Ox} + 4.8\ \mathrm{eV})$$

$$E_{\mathrm{LUMO}} \approx -(E_{1/2}^{Red} + 4.8\ \mathrm{eV})$$

Thereby, all redox potentials were referred to the Fc/Fc^+ couple which was set to 0 V (*vs.* Ag/AgCl).

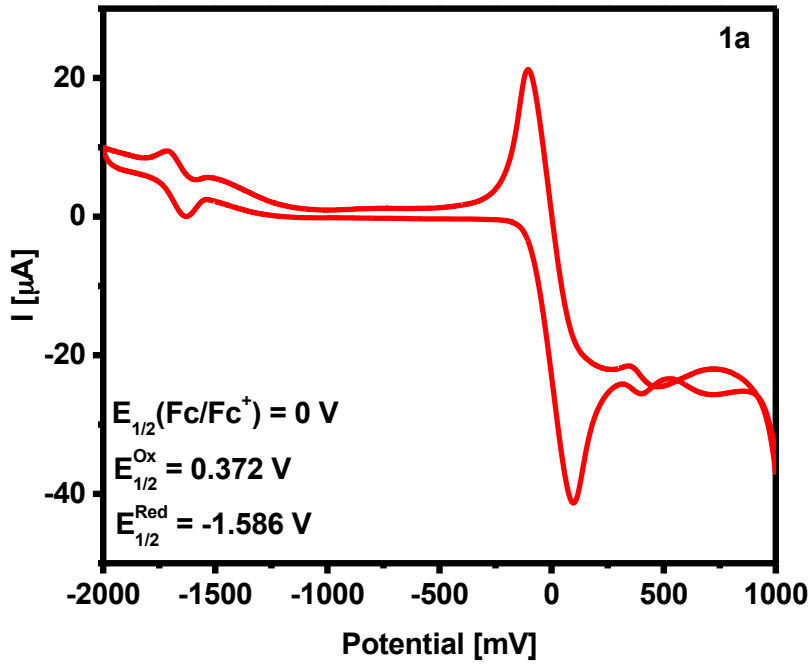

Figure S4: Cyclovoltammogramm of 1a (c= 0.48 mM) in 0.1 M solution *n*-Bu_4NPF_6 in CH_2Cl_2.

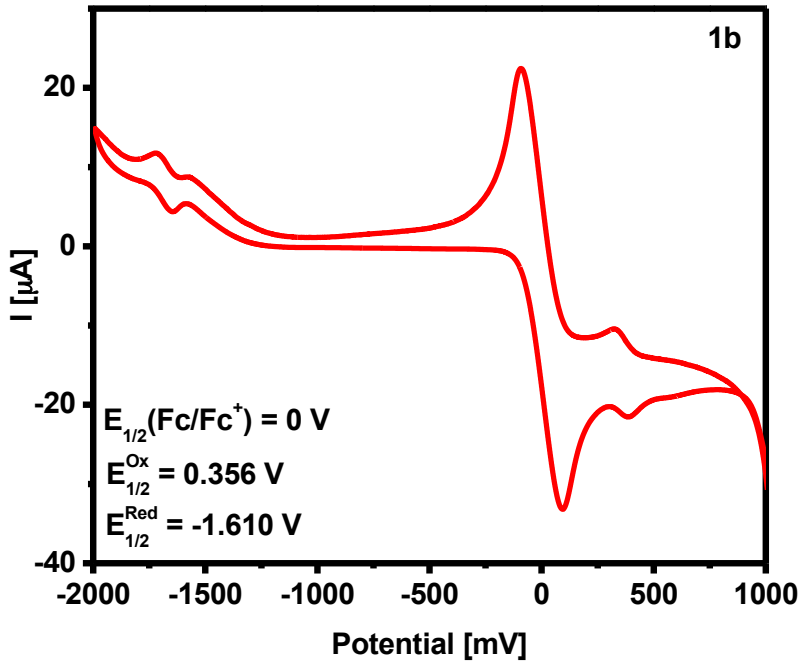

Figure S5: Cyclovoltammogramm of 1b (c= 0.81 mM) in 0.1 M solution *n*-Bu_4NPF_6 in CH_2Cl_2.

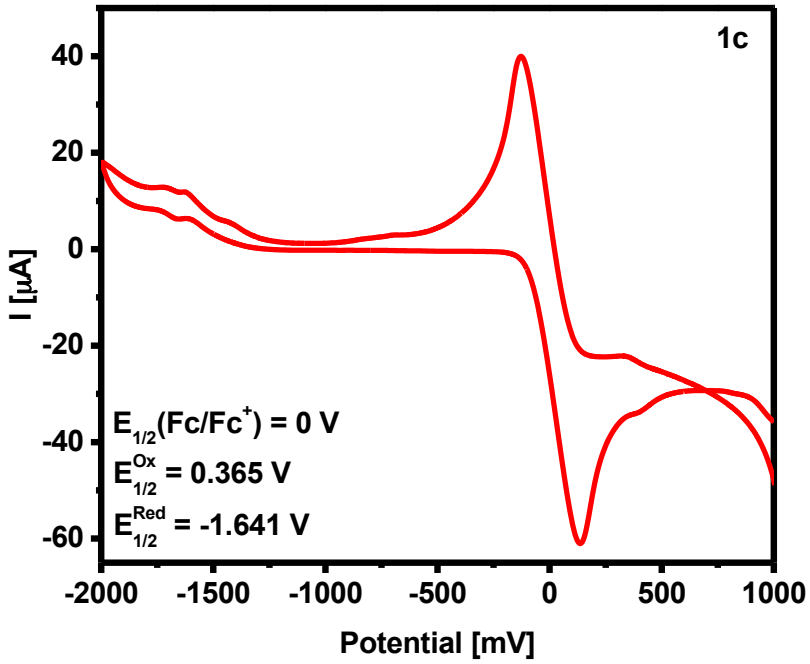

Figure S6: Cyclovoltammogramm of 1c (c= 0.87 mM) in 0.1 M solution *n*-Bu_4NPF_6 in CH_2Cl_2.

5. ^{1}H NMR, ^{13}C NMR, and ^{19}F NMR spectra for Compunds 1a–c:

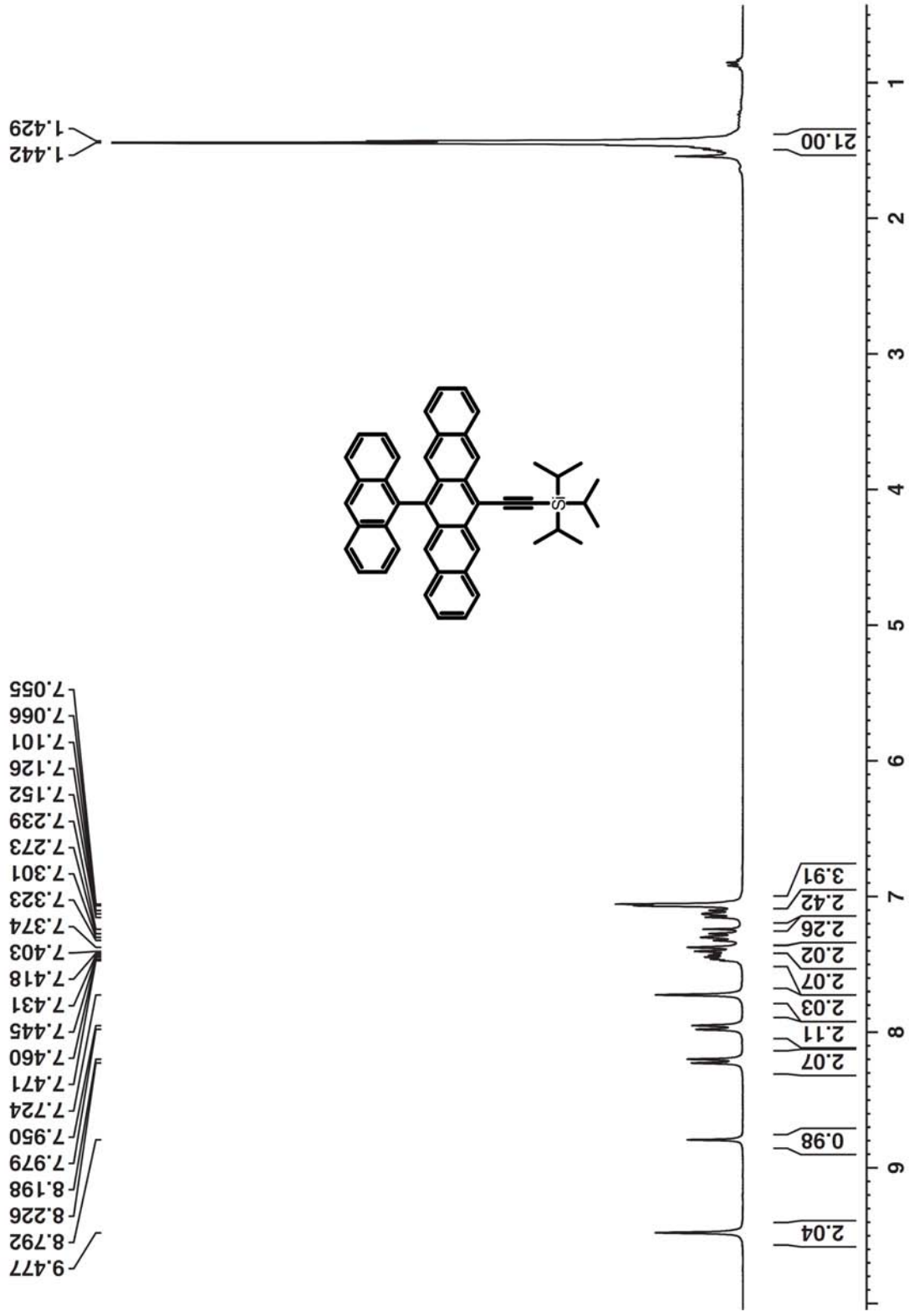

Figure S7: ^{1}H NMR spectrum of 1a in $CDCl_3$, 300 MHz.

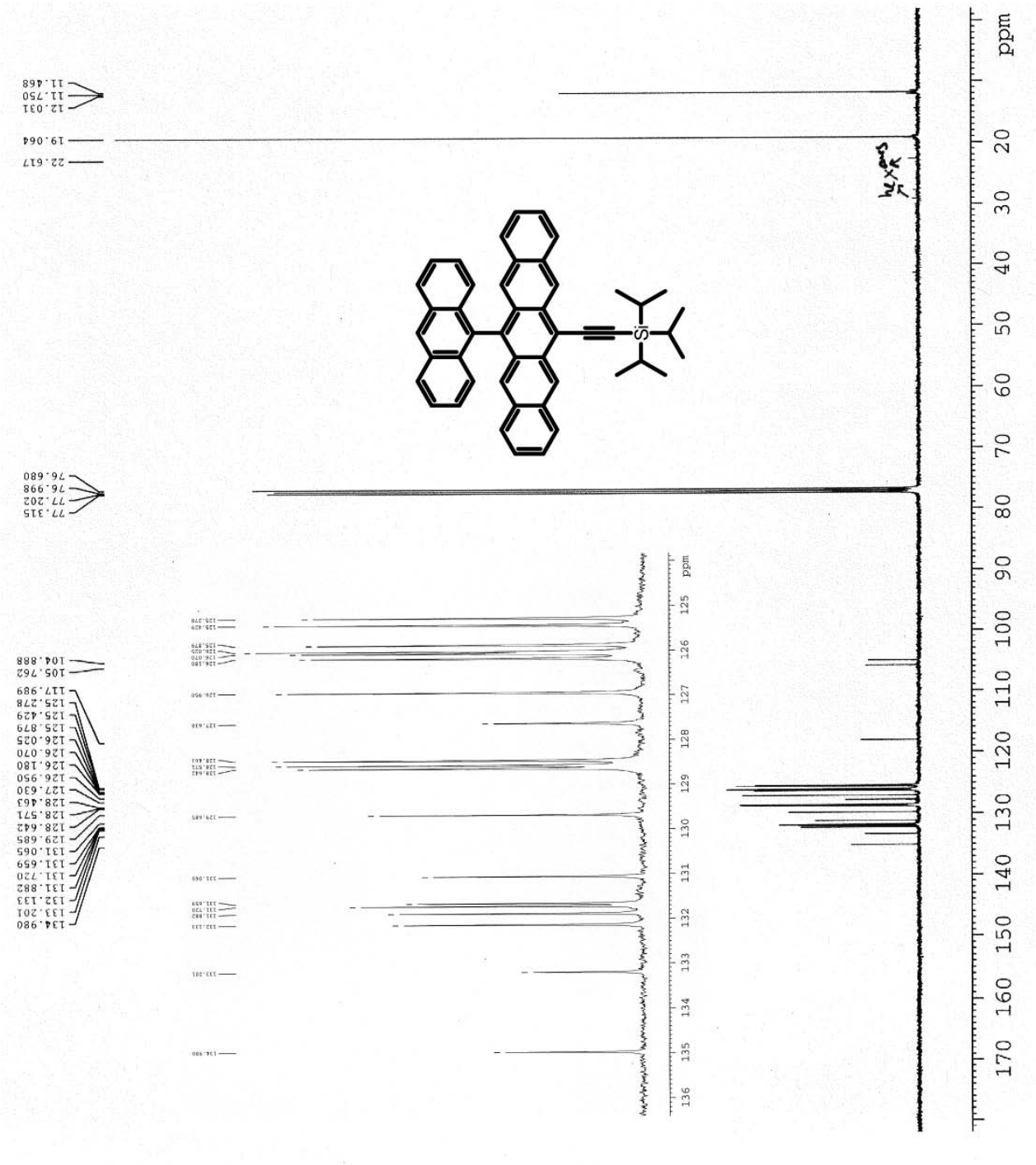

Figure S8: ^{13}C NMR spectrum of 1a in CDCl3, 100.5 MHz.

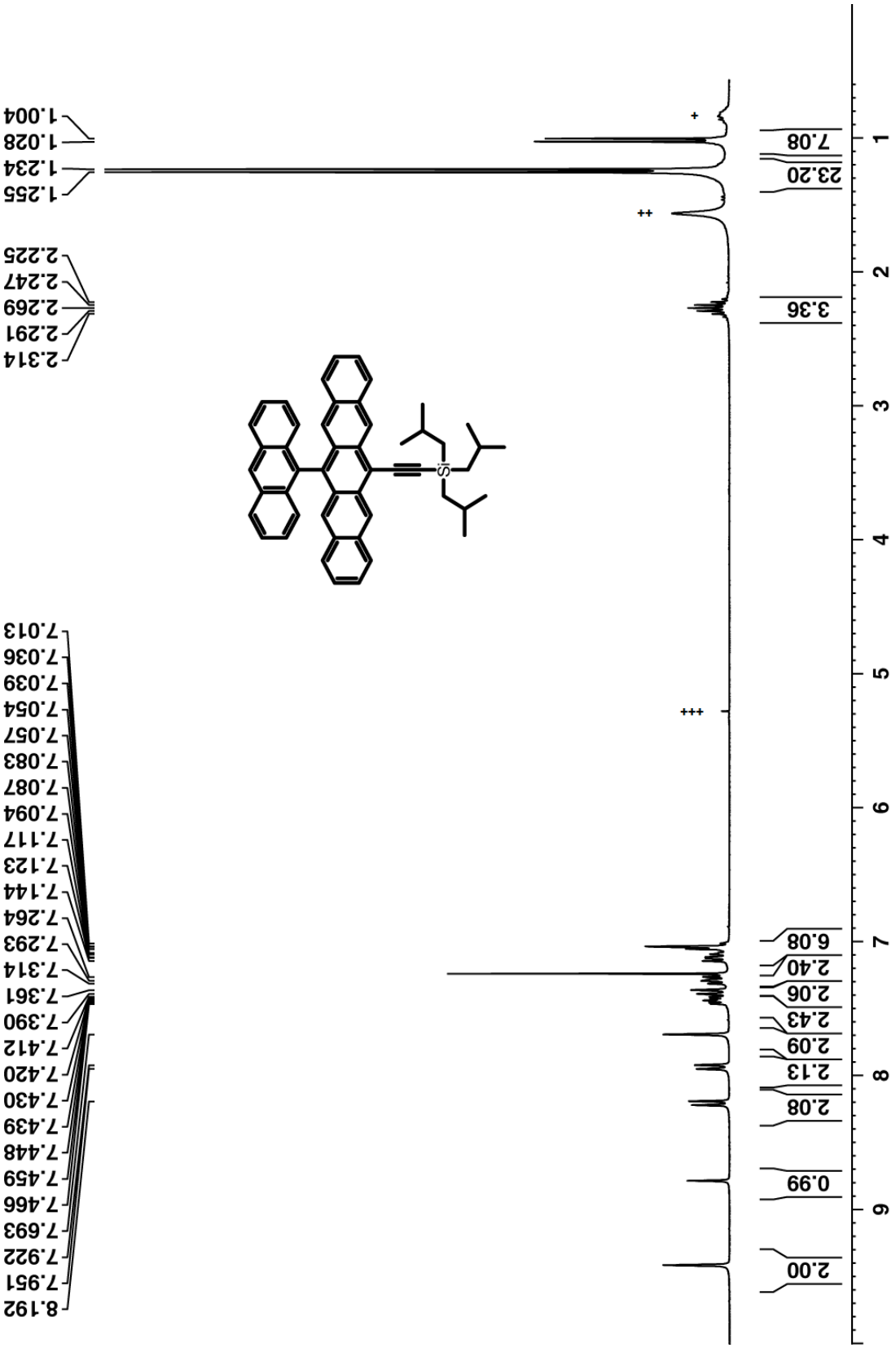

Figure S9: ^{1}H NMR spectrum of 1b in $CDCl_3$, 300 MHz; hexanes (+), H_2O (++), CH_2Cl_2 (+++).

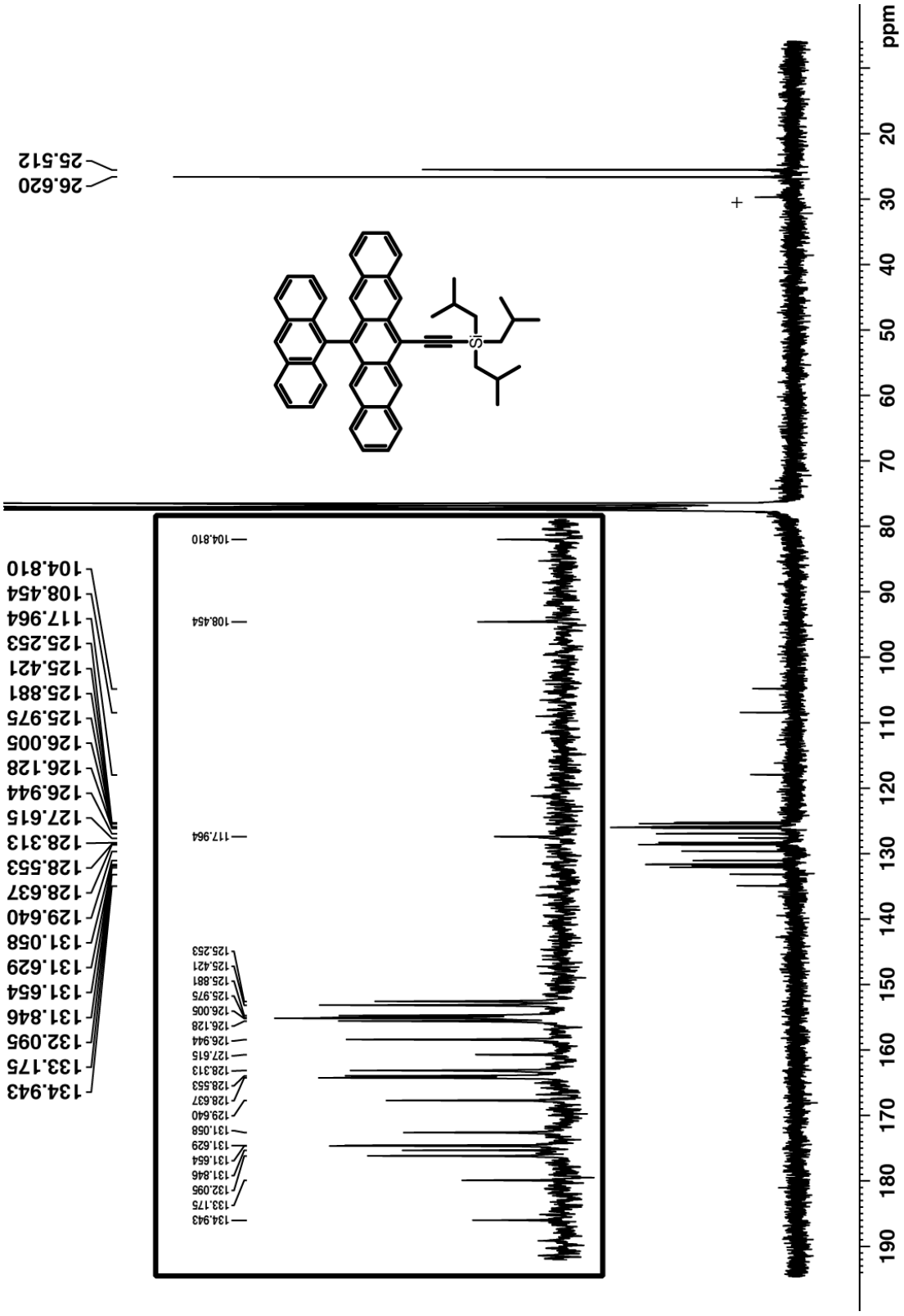

Figure S10: ^{13}C NMR spectrum of 1b in $CDCl_3$, 75.5 MHz; impurity (THF stabilizer) (+).

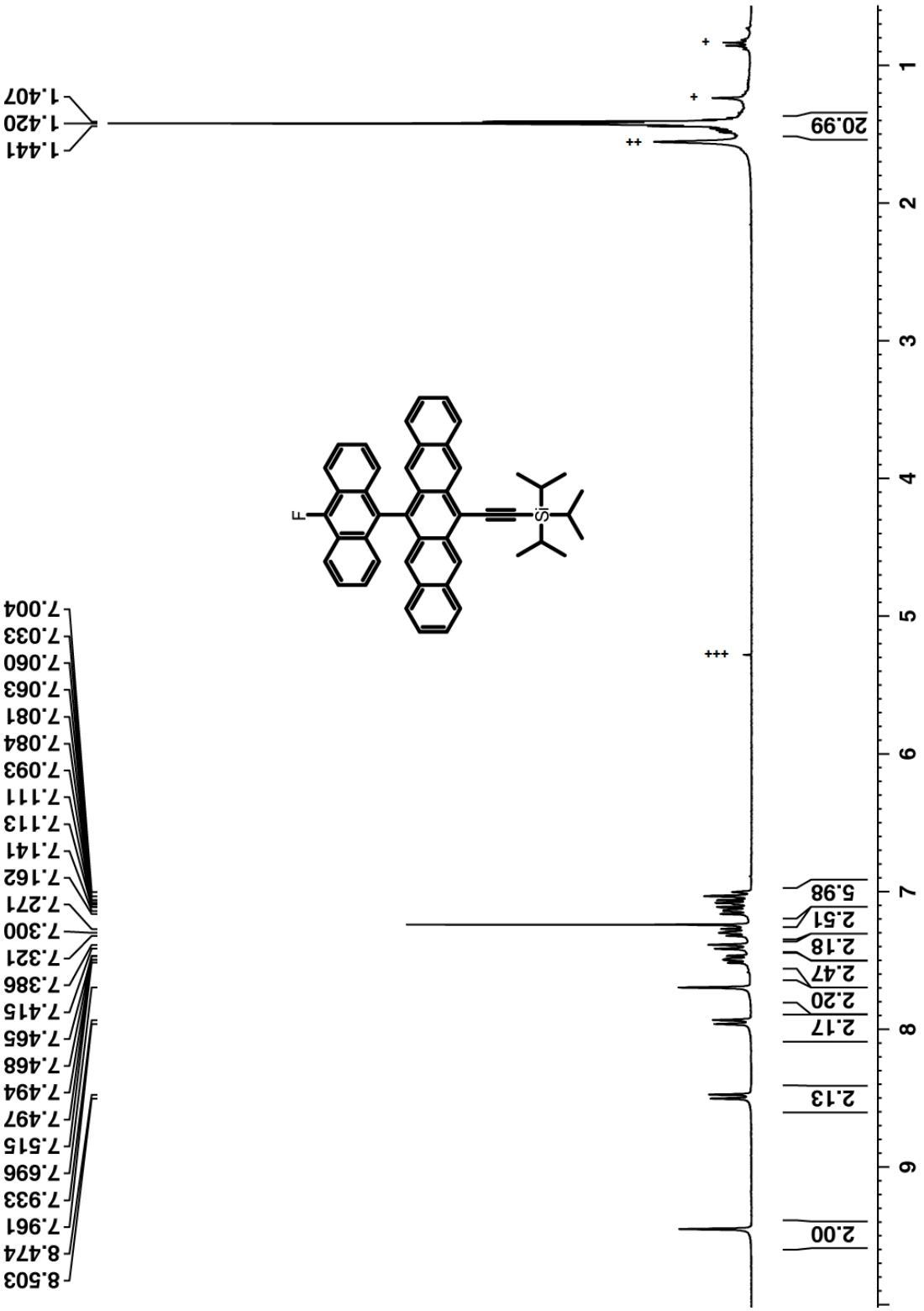

Figure S11: ^{1}H NMR spectrum of 1c in $CDCl_3$, 300 MHz; hexanes (+), H_2O (++), CH_2Cl_2 (+++).

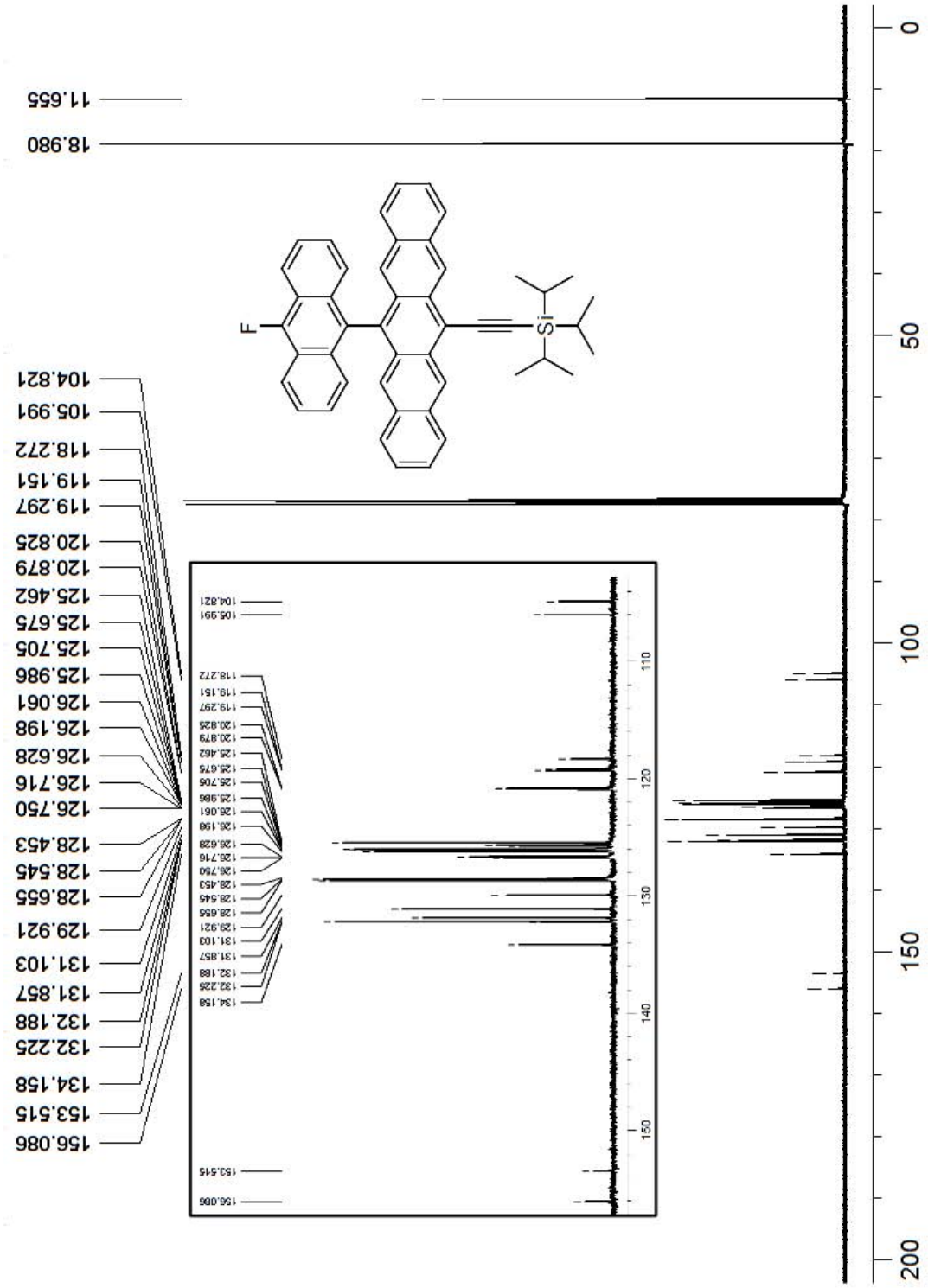

Figure S12: ^{13}C NMR spectrum of 1c in $CDCl_3$, 100.5 MHz.

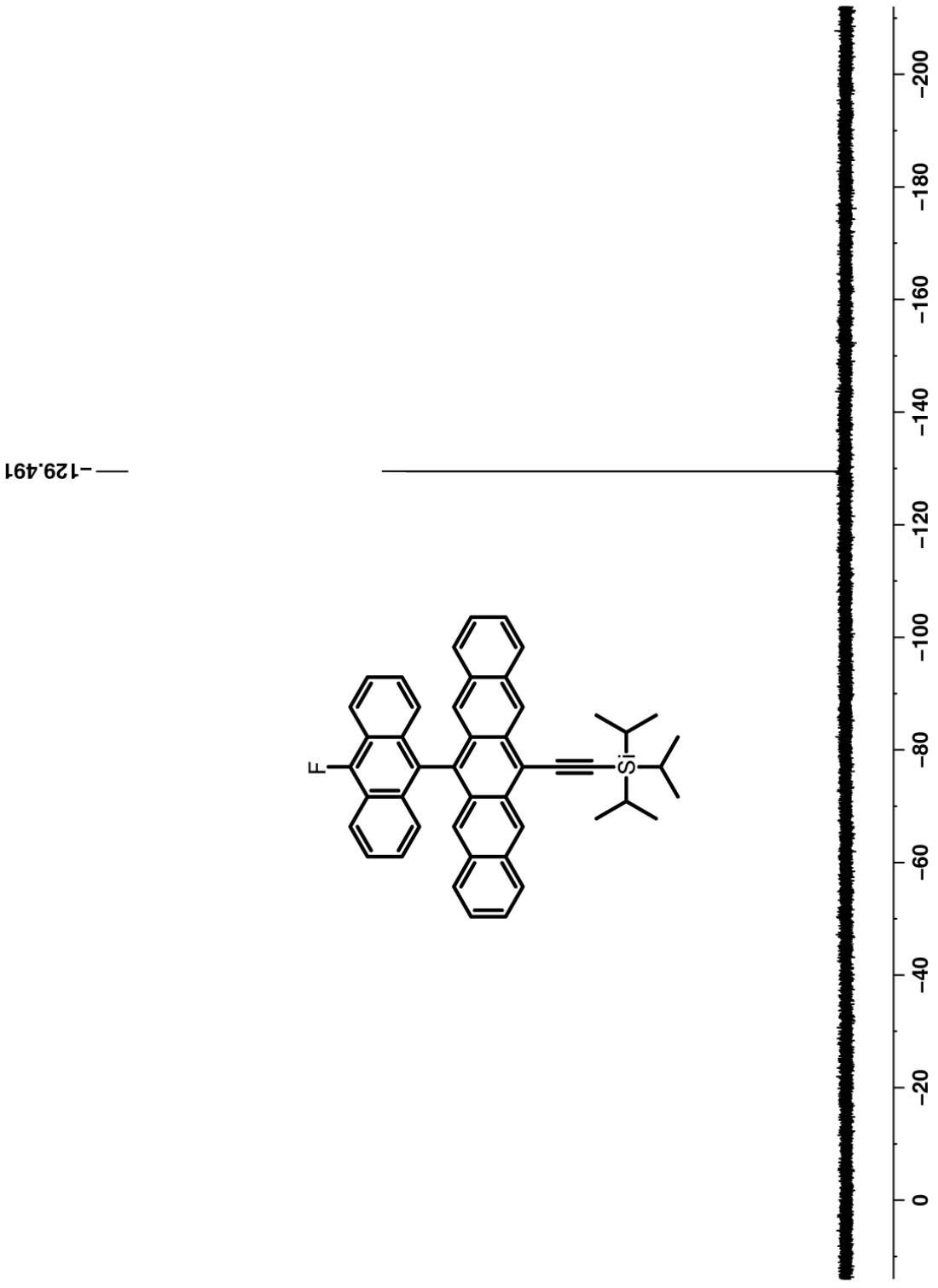

Figure S13: ^{19}F NMR spectrum of 1c in $CDCl_3$, 282 MHz.

6. X-ray Crystallographic Analysis for Compounds 1a–c

a) Unit cells of Compounds 1a–c

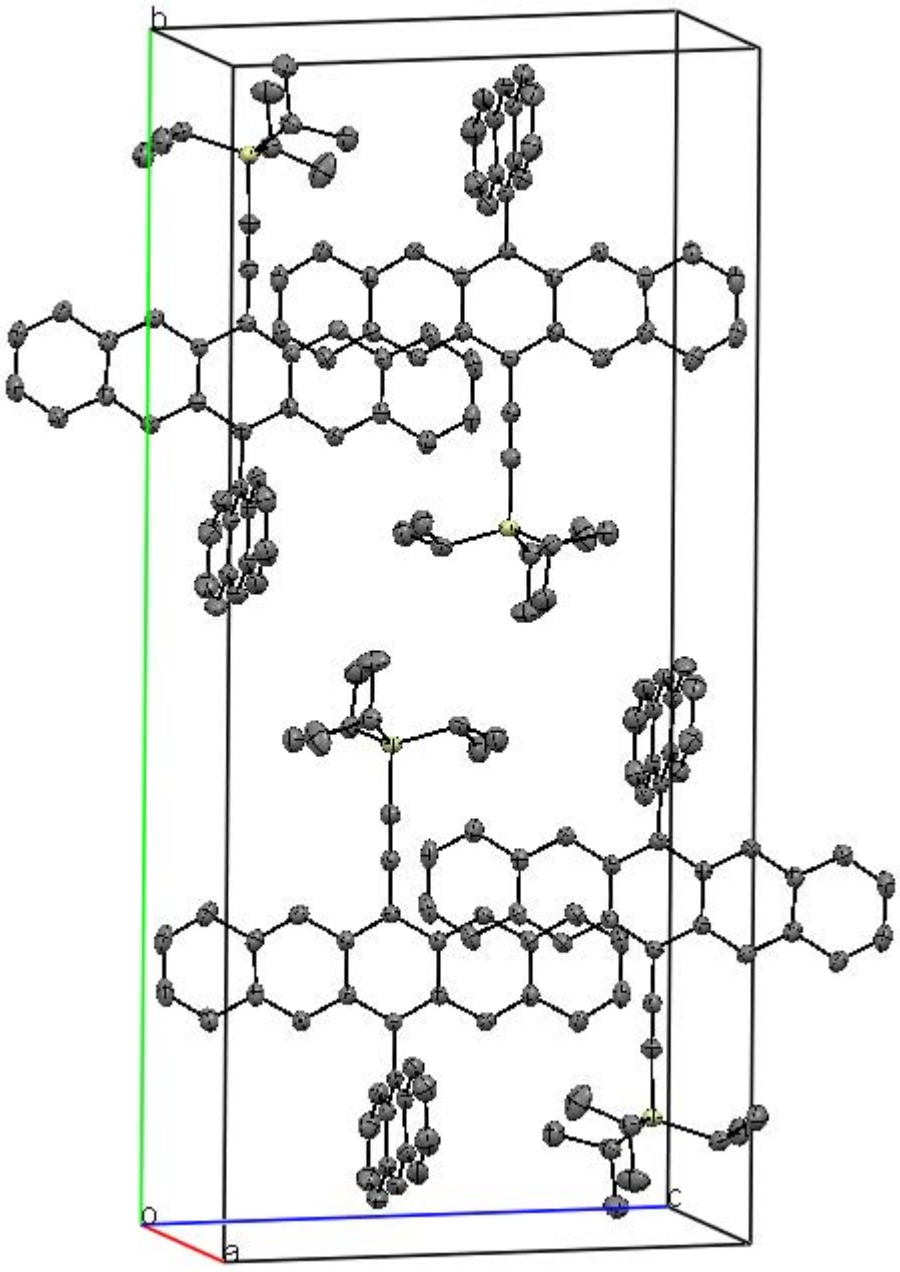

Figure S14: Unit cell of 1a.

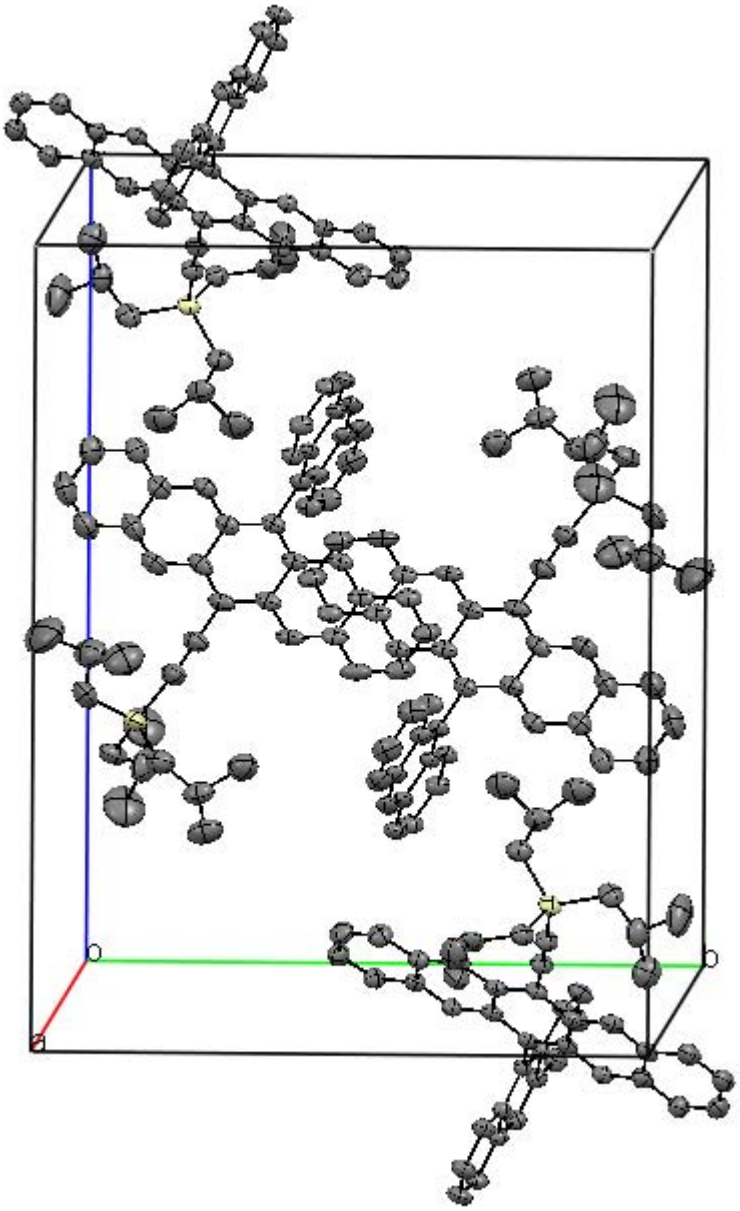

Figure S15: Unit cell of 1b.

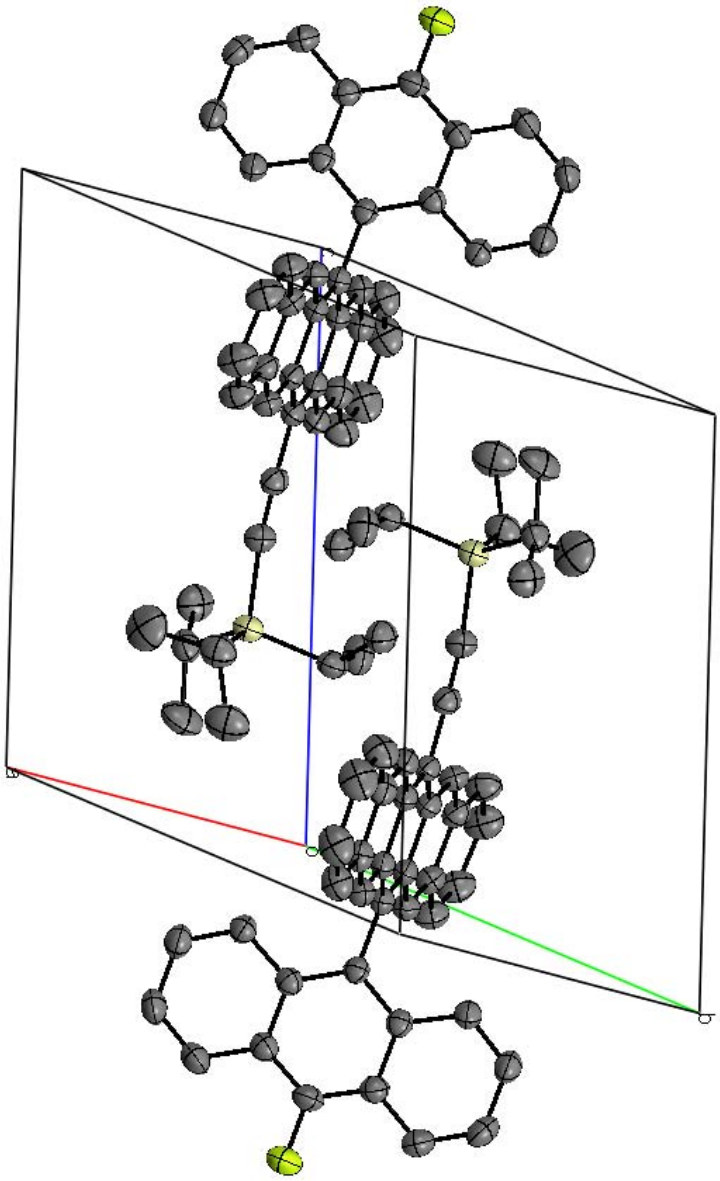

Figure S16: Unit cell of 1c.

b) Packing Diagrams of Compounds 1a–c

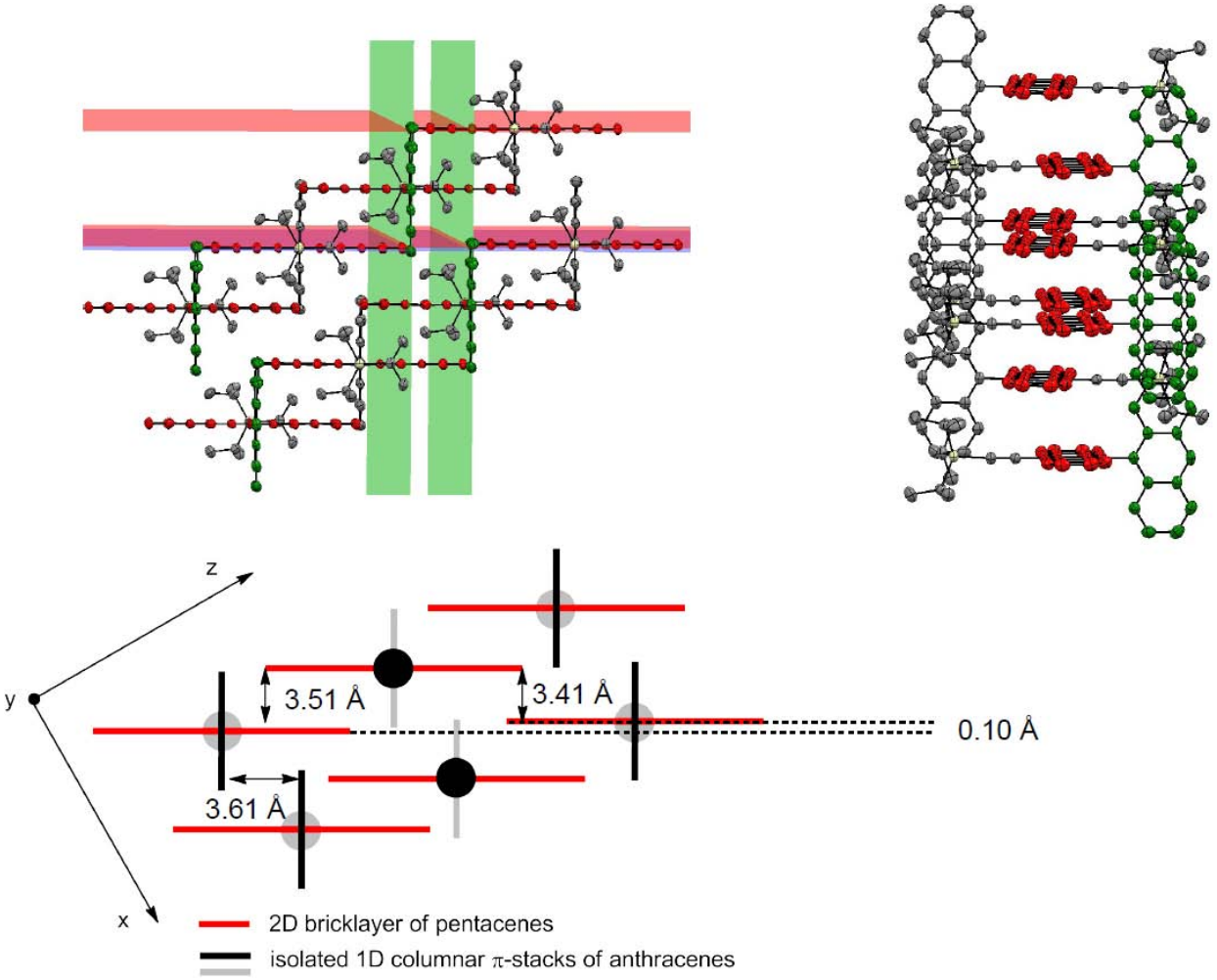

Figure S17: Crystal packing of 1a; 2D bricklayer of pentacenes (red) and separated 1D π-stacks of anthracenes (green or black/grey respectively) viewed from the side and the front; distances were determined by the indicated planes.

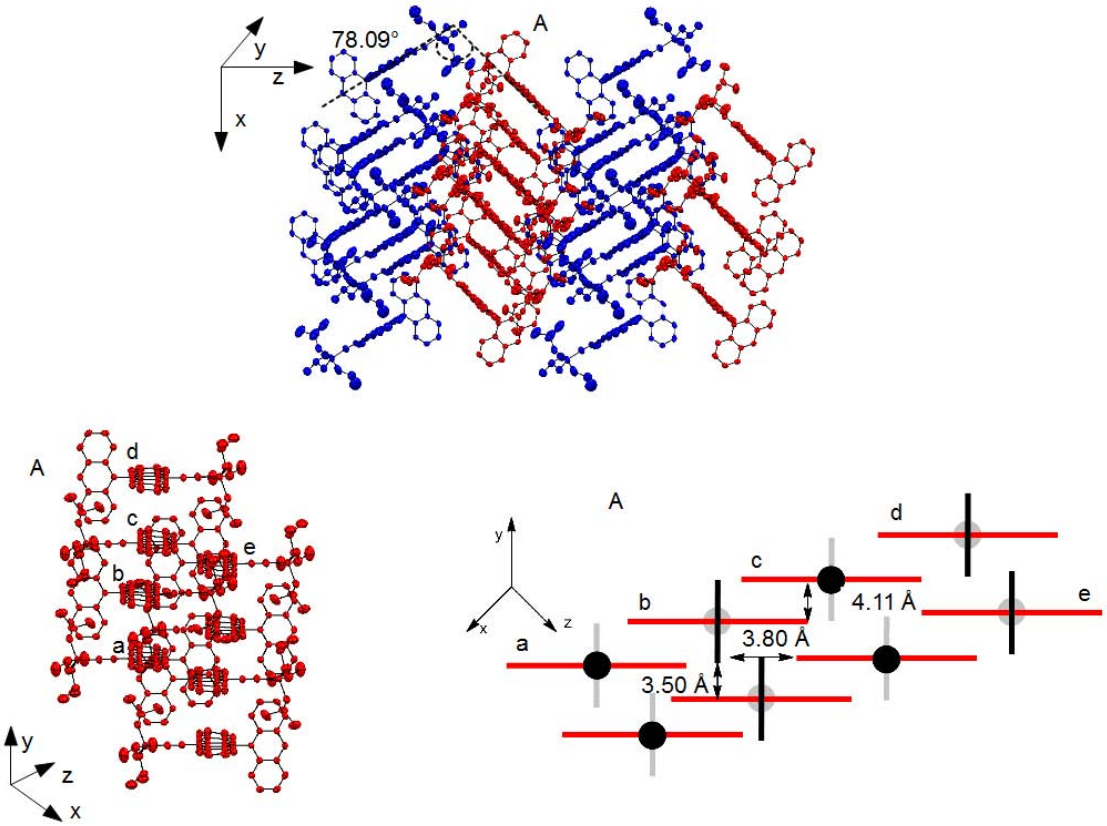

Figure S18: Crystal packing of 1b; herring-bone arrangement of separated 1D π-stacks; characteristic distances were determined by planes parallel to the according acene unit.

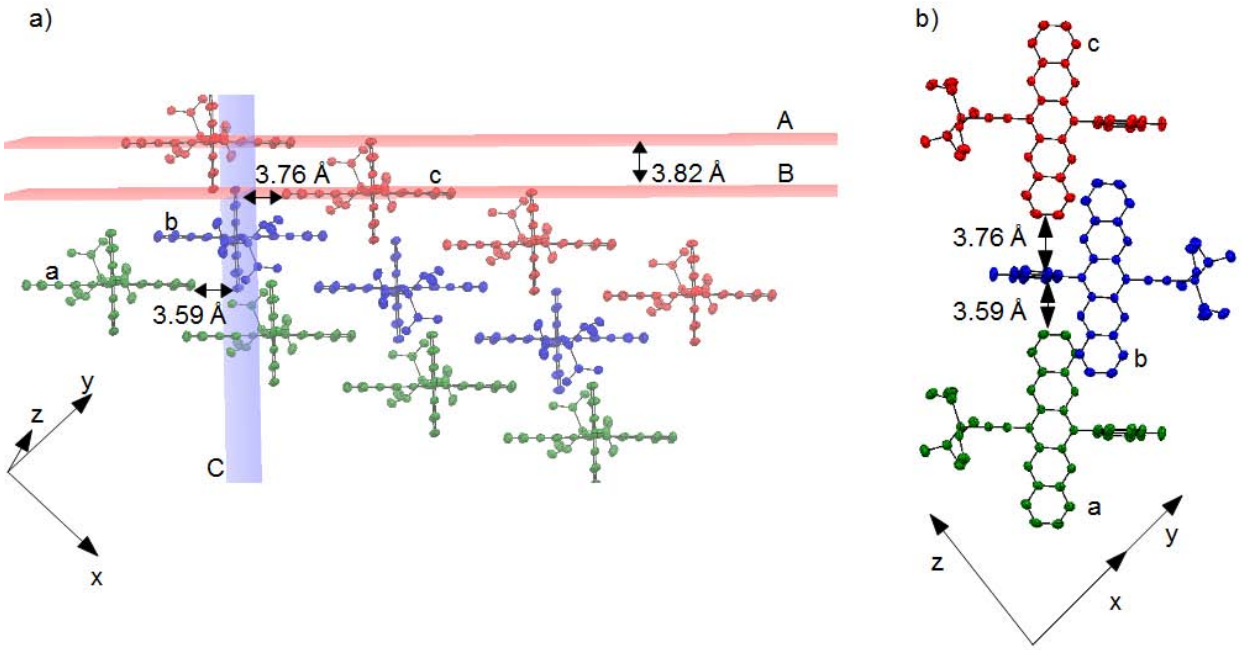

c)

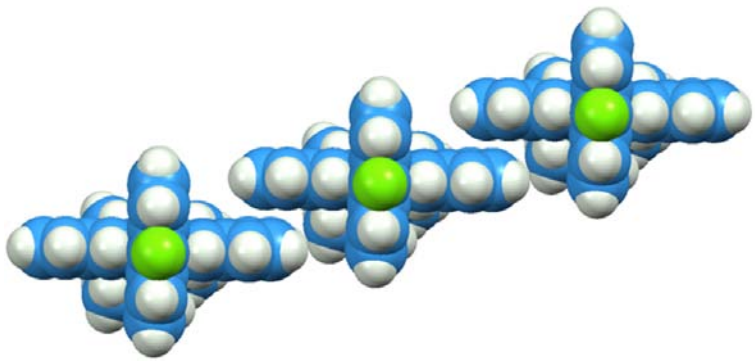

Figure S19: a) Crystal packing of 1c; the different colors indicate the individual 1D π-stacks; the characteristic distances were determined by the indicated planes. b) Molecules a, b, and c viewed from the top; Molecules a and c are associated to molecule b by edge-to-face interactions, leading to periodic steps between the 1D π-stacks. c) Space filling representation of intermolecular packing of neighboring molecules in the 1D slipped stacks (Carbon = blue, Hydrogen = white, and Fluorine = green).

7. Transistor Device Fabrication

All devices were fabricated by vapor phase depostition of Al, the organic material, and Au. An Leybold Sytems Univex 300 was used for the organic material and a customized vacuum chamber was used for Al and Au. The O_2 plasma treatment was carried out, using a Diener Electronic Pico plasma generator. For the SAM treatment, a Chemat Technology Inc. Modelkw-4AH hotplate was used. Static contact angles of water were determined, using a Dataphysics contact angle system OCA30.

All transistor devices were fabricated on heavily doped Si wafers with a 100 nm layer thermally grown SiO_2 on top. All devices are arranged in a bottom gate top contact architecture with channel lengths from L = 20 µm to L = 300 µm and a constant channel width of W = 500 µm. *Iso*-propanol and tetradecyl-phosphonic acid (C_{14}PA, PCI Synthesis) were used as received. For the devices using an Al gate electrode, a 30 nm thick Al layer was deposited by vapor phase deposition, at 10^{-7} mbar with a rate of 3.5 Å/s. The gate dielectric was created by O_2 plasma treatment at 0.2 mbar O_2 atmosphere. This creates an AlO_x layer of about 3.6 nm.[4] The C_{14} PA SAM was deposited onto the AlO_x gate dielectric by immersion of the corresponding wafer in an 0.26 mM solution of C_{14}-PA in *iso*-propanol for 24 h. Afterwards, the wafer was rinsed twice with *iso*-propanol and treated on a hotplate at 60 °C for 3 min, to yield a densely packed SAM.[5] The successful formation of the SAM was proven by static contact angle measurement with water, yielding angles of about 112° for the C_{14}PA SAM. The corresponding organic semiconductor was deposited from the vapor phase at 10^{-6} mbar and a rate of about 0.1 Å/s at a substrate temperature of 80 °C during deposition of the semiconductor. The source and drain electrodes were made by vapor phase deposition of Au at 10^{-6} mbar at a rate of 1.5 Å/s. Patterning of the devices was achieved by alignment of a shadow mask with channel width of W = 500 µm and channel lengths reaching from L = 20 µm to L = 300 µm. Capacitors (Al/AlO_x–C_{14}-PA/Au; 50 µm x 50 µm) were fabricated on different wafers, using the same process parameters. The determined capacitance of 0.72 µF/cm^2 corresponds to those determined in previous studies.[6] For the devices using a Si gate electrode and SiO_2 gate dielectric, the Si/SiO_2 wafers were used as received. The deposition of the organic material and the Au was done as described above. During the entire fabrication process, OTFT structures, with the semiconductor **1a**–**c** already deposited, were not exposed to air for longer than 30 min. After approximately one week under ambient conditions, the OTFT devices no longer showed transistor behavior any more. When kept under inert atmosphere and protected from light, the OTFT still worked after nine month of storage.

8. Electrical Characterization of Transistors and AFM data

The electrical characterization of all fabricated transistor devices was performed in a glove-box (Jacomex) under N_2 atmosphere. Thereby, a precision semiconductor parameter analyzer 4156C (Agilent), mounted on a vibration isolation system (Newport) was used. All transfer characteristics were measured in steps of 50 mV and by scanning from positive to negative bias with 2 s hold between the sweeps. The reported charge carrier mobilities in the saturation regime were determined according the gradual channel approximation, by using the equation:

$$\mu = \left(\frac{\partial\sqrt{I_D}}{\partial V_G}\right)^2 \cdot \frac{2L}{W \cdot C_i}$$

with $\left(\frac{\partial\sqrt{I_D}}{\partial V_G}\right)$ being slope of the plot $\sqrt{I_D}$ *versus* V_G in the transfer plot of the saturation regime, *L* being the channel length, *W* being the channel width and C_i being the capacitance of the dielectric material. Capacitances were determined at a frequency of 100 kHz, using a semiconductor parameter analyzer B1500 (Agilent) under ambient conditions.

Table 1: Electrical characterization of the Si/SiO_2 OTFTs in the p-type direction (each entry represents the mean value calculated from at least three devices with the same *W* and *L* dimensions).

	μ_{sat} [cm^2/Vs]	V_{th} [V]	I_{on} / I_{off}	I_D / I_G	*L* [µm]	*W* [µm]
1a	$1.2\cdot10^{-7}$	−19.6	$2.6\cdot10^{1}$	$1.5\cdot10^{1}$	100	500
1b	$7.1\cdot10^{-7}$	−5.6	$3.7\cdot10^{2}$	$2.0\cdot10^{2}$	100	500
1c	$6.8\cdot10^{-7}$	−10.8	$7.6\cdot10^{2}$	$3.5\cdot10^{2}$	100	500

Table 2: Electrical characterization of the AlO_x-C_{14}PA hybrid gate dielectric OTFTs (each entry represents the mean value calculated from at least four devices with the same *W* and *L* dimensions).

	μ_{sat} [cm^2/Vs]	V_{th} [V]	I_{on} / I_{off}	I_D / I_G	*L* [µm]	*W* [µm]
1b	$1.8\cdot10^{-2}$	−1.9	$7.5\cdot10^{3}$	$1.4\cdot10^{1}$	60	500
1c - holes	$1.6\cdot10^{-1}$	−1.9	$9.1\cdot10^{4}$	$9.2\cdot10^{2}$	60	500
1c - electrons	$7.6\cdot10^{-3}$	2.6	$3.8\cdot10^{3}$	$5.2\cdot10^{0}$	60	500

Table 3: Electrical characterization of the AlO_x-C_{14}PA hybrid dielectric OTFTs (each entry represents the mean value calculated from at least three devices with the same *W* and *L* dimensions).

	μ_{sat} [cm^2/Vs]	V_{th} [V]	I_{on} / I_{off}	I_D / I_G	*L* [µm]	*W* [µm]
1b	$3.7\cdot10^{-2}$	−2.1	$4.4\cdot10^{4}$	$3.0\cdot10^{1}$	80	500
1c - holes	$8.3\cdot10^{-2}$	−1.8	$3.3\cdot10^{4}$	$2.5\cdot10^{2}$	80	500
1c - electrons	$1.2\cdot10^{-2}$	2.7	$2.0\cdot10^{3}$	$2.7\cdot10^{0}$	80	500

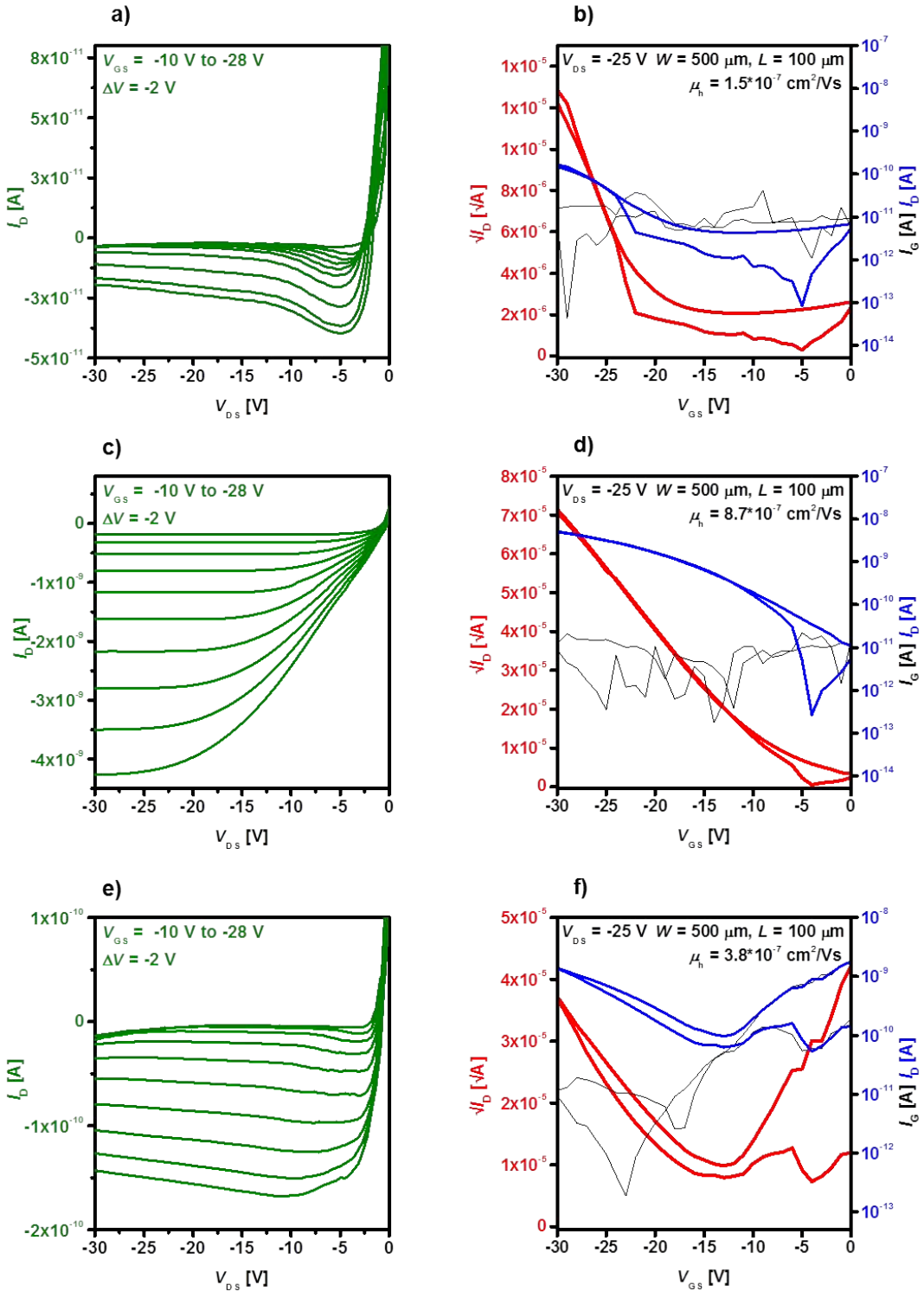

Figure S20: Output (a) and transfer (b) characteristics of an Si/SiO_2 OTFT using 1a as semiconductor, V_{th} = –19.4 V, I_{on} / I_{off} = 3.8·10^1, I_D / I_G = 2.1·10^1; Output (c) and transfer (d) characteristics of an Si/SiO_2 OTFT using 1b as semiconductor, V_{th} = –6.1 V, I_{on} / I_{off} = 4.6·10^2, I_D / I_G = 2.4·10^2; c) Output (e) and transfer (f) characteristics of an Si/SiO_2 OTFT using 1c as semiconductor, V_{th} = –11.6 V, I_{on} / I_{off} = 2.0·10^1, I_D / I_G = 1.5·10^2.

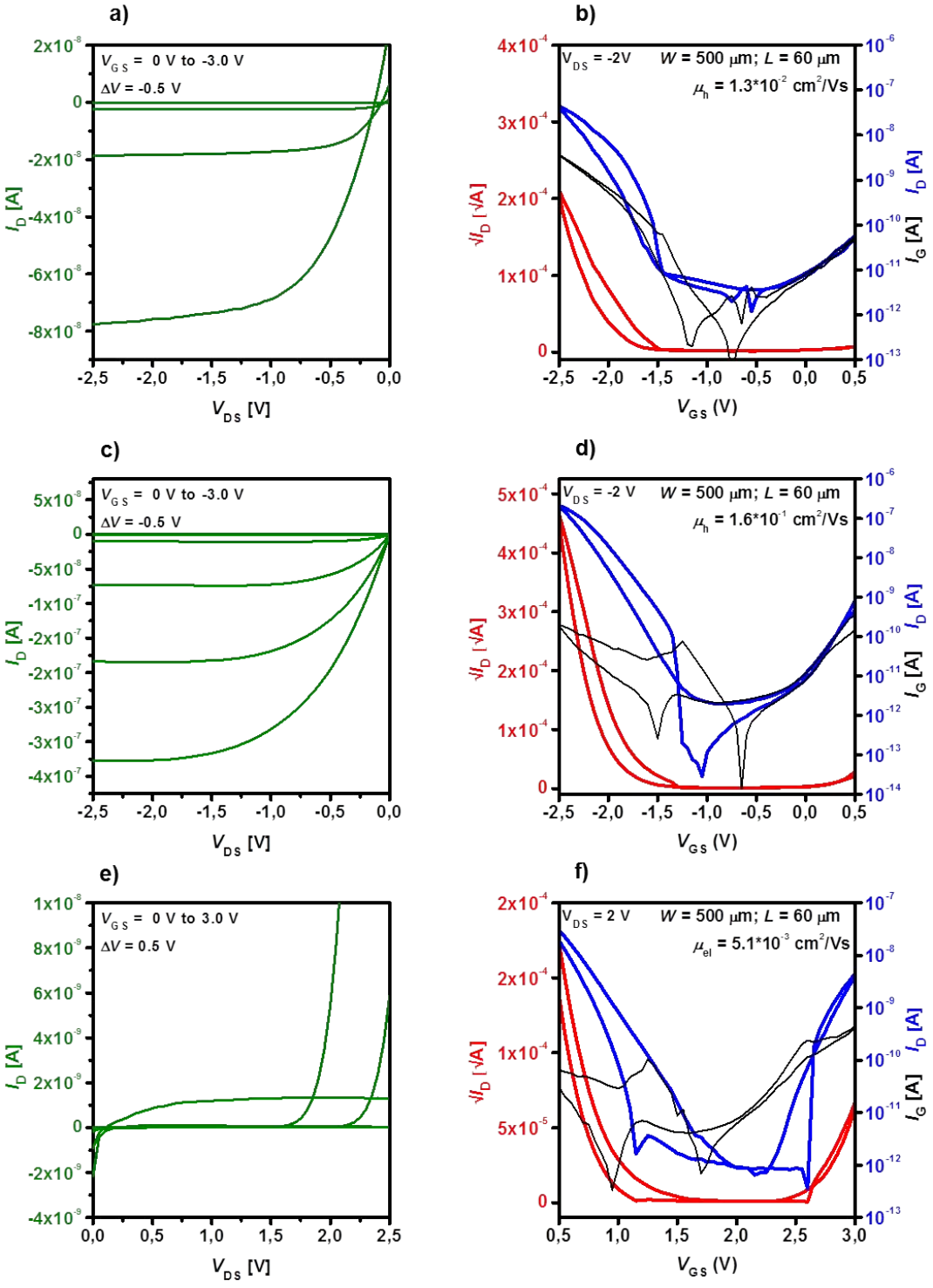

Figure S21: Output (a) and transfer (b) characteristics of an AlO_x-C_{14}PA hybrid dielectric OTFT using 1b as semiconductor, V_{th} = –1.6 V, I_{on} / I_{off} = 1.5·10^4, I_D / I_G = 1.2·10^1; Output (c) and transfer (d) characteristics in p-direction of an AlO_x-C_{14}PA hybrid dielectric OTFT using 1c as semiconductor, V_{th} = –1.8 V, I_{on} / I_{off} = 1.1·10^5, I_D / I_G = 1.1·10^3; Output (e) and transfer (f) characteristics in n-direction of an AlO_x-C_{14}PA hybrid dielectric OTFT using 1c as semiconductor, V_{th} = 2.5 V, I_{on} / I_{off} = 4.0·10^3, I_D / I_G = 1.0·10^1.

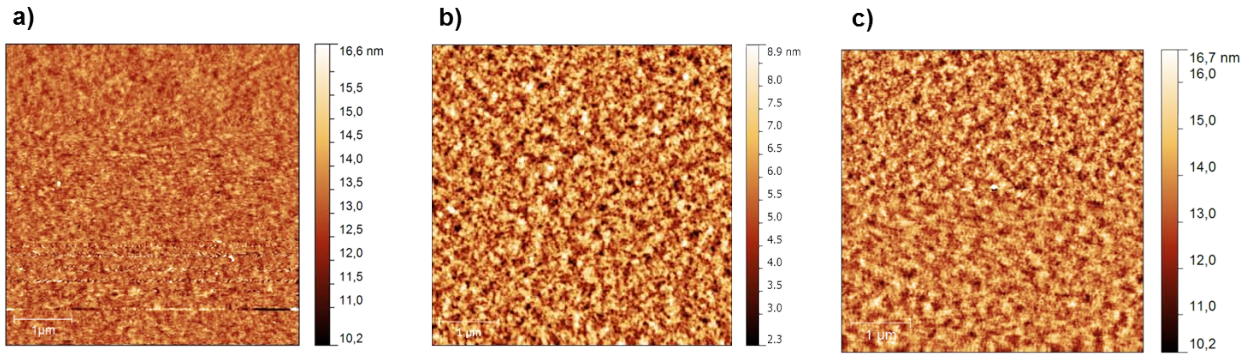

Figure S22: AFM data of a 20 nm film of 1a (a), 1b (b), and 1c (c) on the SiO_2 gate dielectric.

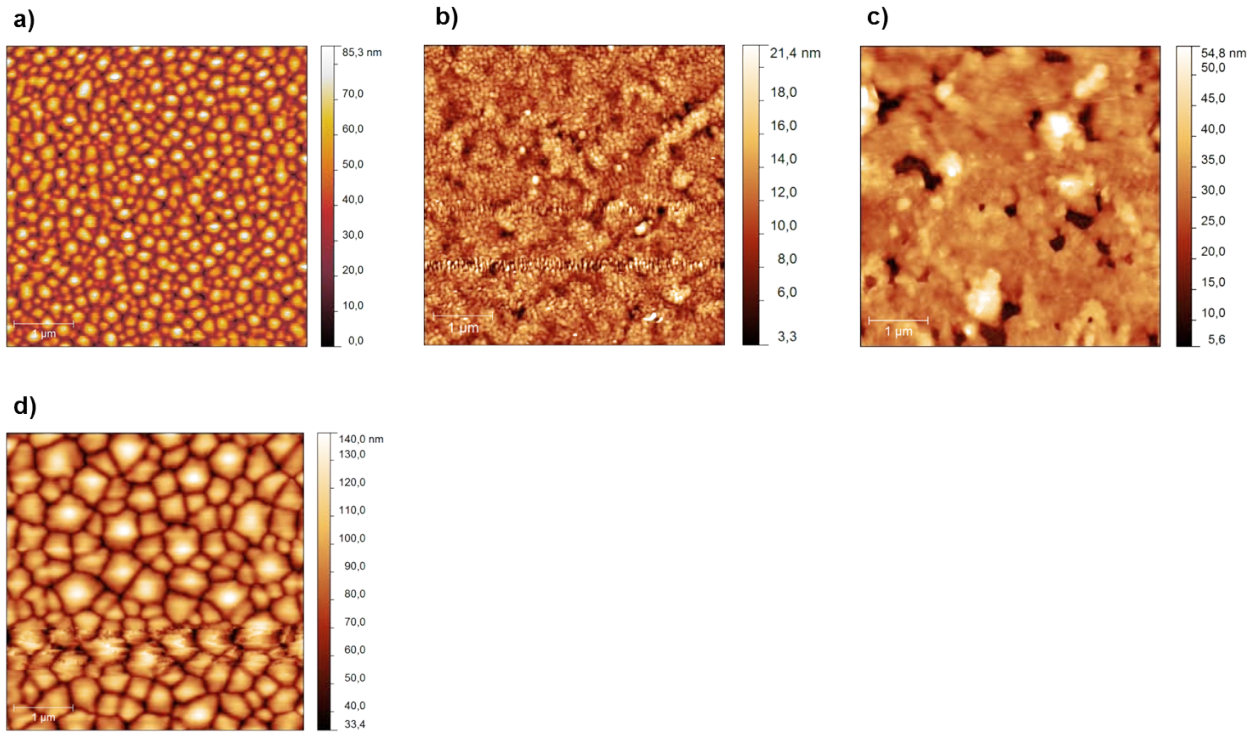

Figure S23: AFM data of a 20 nm film of 1a (a), 1b (b), and 1c (c) on the AlO_x-C_{14}PA hybrid gate dielectric; (d) AFM data of 30 nm of 1a on the AlO_x-C_{14}PA hybrid gate dielectric.

References:

1 L. Zhu, R. O. Al-Kaysi, R. J. Dillon, F. S. Tham, C. J. Bardeen, *Cryst. Grow. Des*. 2011, **11**, 4975–4983.

2 D. Lehnherr, A. H. Murray, R. McDonald, R. R. Tykwinski, *Angew. Chem. Int. Ed*. 2010, **49**, 6190–6194; D. Lehnherr, J. Gao, F. A. Hegman, R. R. Tykwinski, *Org. Lett*. 2008, **10**, 4779–4782.

3 J. Pommerehne, H. Vestweber, W. Guss, R. F. Mahrt, H. Bässler, Porsch Michael, J. Daub, *Adv. Mater.* **1995**, *7*, 551–554.

4 M. Novak, A. Ebel, T. Meyer-Friedrichsen, A. Jedaa, B. F. Vieweg, G. Yang, K. Voitchovsky, F. Stellacci, E. Spiecker, A. Hirsch, M. Halik, *Nano Lett*. 2011, **11**, 156–159.

5 M. Novak, T. Schmaltz, H. Faber, M. Halik, *Appl. Phys. Lett.* 2011, **98**, 093302.

6 M. Salinas, C. M. Jäger, A. Y. Amin, P. O. Dral, T. Meyer-Friedrichsen, A. Hirsch, T. Clark, M. Halik, *J. Am. Chem. Soc.* 2012, **134**, 12648–12652.